Soft Matter

PAPER

View Article Online
View Journal | View Issue

Cite this: *Soft Matter*, 2015, **11**, 3003

Fusion of raft-like lipid bilayers operated by a membranotropic domain of the HSV-type I glycoprotein gH occurs through a cholesterol-dependent mechanism†

Giuseppe Vitiello,[ab] Annarita Falanga,[c] Ariel Alcides Petruk,[d] Antonello Merlino,[ef] Giovanna Fragneto,[g] Luigi Paduano,[be] Stefania Galdiero[c] and Gerardino D'Errico*[be]

Received 12th December 2014
Accepted 19th February 2015

DOI: 10.1039/c4sm02769h

www.rsc.org/softmatter

A wealth of evidence indicates that lipid rafts are involved in the fusion of the viral lipid envelope with the target cell membrane. However, the interplay between these sterol- and sphingolipid-enriched ordered domains and viral fusion glycoproteins has not yet been clarified. In this work we investigate the molecular mechanism by which a membranotropic fragment of the glycoprotein gH of the Herpes Simplex Virus (HSV) type I (gH625) drives fusion of lipid bilayers formed by palmitoyl oleoyl phosphatidylcholine (POPC)–sphingomyelin (SM)–cholesterol (CHOL) (1 : 1 : 1 wt/wt/wt), focusing on the role played by each component. The comparative analysis of the liposome fusion assays, Dynamic Light Scattering (DLS), spectrofluorimetry, Neutron Reflectivity (NR) and Electron Spin Resonance (ESR) experiments, and Molecular Dynamics (MD) simulations shows that CHOL is fundamental for liposome fusion to occur. In detail, CHOL stabilizes the gH625-bilayer association by specific interactions with the peptide Trp residue. The interaction with gH625 causes an increased order of the lipid acyl chains, whose local rotational motion is significantly hampered. SM plays only a minor role in the process, favoring the propagation of lipid perturbation to the bilayer inner core. The stiffening of the peptide-interacting bilayer leaflet results in an asymmetric perturbation of the membrane, which is locally destabilized thus favoring fusion events. Our results show that viral fusion glycoproteins are optimally suited to exert a high fusogenic activity on lipid rafts and support the relevance of cholesterol as a key player of membrane-related processes.

1 Introduction

Lipid rafts are nanosized, dynamic sterol- and sphingolipid-enriched domains of the plasma membrane, which present reduced fluidity and permeability.[1,2] Since their discovery, rafts have been recognized as the preferential localization region of a variety of membrane proteins. Consequently, they have been proposed to be involved in many physiologic or pathologic cellular processes based on a combination of lipid–protein, protein–protein and lipid–lipid interactions, including T and B cell activation,[3] cell adhesion,[4] membrane trafficking in epithelial cells,[5] and amyloid β peptide fibrillogenesis.[6]

Many studies have suggested the critical role of lipid rafts in infections by enveloped viruses. In particular, the involvement of lipid rafts has been demonstrated in different stages of the viral life cycle.[7–9] For enveloped viruses, entry and egress from the target cells require a sequence of fusion and fission events between the viral envelope and the cell membranes. These processes are controlled by one or more viral glycoproteins (fusion proteins) that undergo conformational changes favoring lipid re-arrangement.[10] Studies have suggested that lipid rafts may promote virus entry by concentrating the viral receptors and facilitating binding *via* an efficient interaction of these receptors with viral glycoproteins.[11] In other cases, a physical association of these glycoproteins and membrane lipid micro-domains has been reported to play a key role in promoting the

[a]*Department of Chemical, Materials and Production Engineering, University of Naples "Federico II", Piazzale Tecchio 80, 80125 Naples, Italy*

[b]*CSGI, Consorzio interuniversitario per lo sviluppo dei Sistemi a Grande Interfase, via della Lastruccia 3, SestoFiorentino, 50019, Florence, Italy*

[c]*Department of Pharmacy, DFM Scarl and Centro Interuniversitario di Ricerca sui Peptidi Bioattivi, University of Naples "Federico II", Via Mezzocannone 16, 80134, Naples, Italy*

[d]*Departamento de Quimica Inorganica, Analitica y Quimica Fisica/INQUIMAE-CONICET, University of Buenos Aires, Buenos Aires, Argentina*

[e]*Department of Chemical Sciences, University of Naples "Federico II", Monte Sant'Angelo, 80126, Naples, Italy. E-mail: gerardino.derrico@unina.it; Fax: +39 081 674090; Tel: +39 081 674248*

[f]*Istituto di Biostrutture e Bioimmagini – CNR, Via Mezzocannone 16, 80134, Naples, Italy*

[g]*Institut Laue-Langevin, BP 156, 38042 Grenoble, France*

† Electronic supplementary information (ESI) available. See DOI: 10.1039/c4sm02769h

viral fusion process.[12] Raft-dependent cell entry has been proposed for a variety of enveloped viruses, including HIV,[13] ebola and marburg filoviruses,[14,15] influenza virus,[16] and Newcastle disease virus.[17] In some of these cases the major role has been suggested to be specifically played by cholesterol (CHOL),[13,17] while the relevance of the other raft components has not been clearly identified.

Recent studies have highlighted the role played by rafts and raft-located proteins in the cell entry operated by herpes simplex virus (HSV).[18–20] HSV requires the concerted action of four glycoproteins, named gB, gD, gH, and gL, to execute fusion between the viral envelope and the non-covalently associated plasma membrane of the target cell during the infection process.[21] The crystal structure of the gH–gL complex reveals a boot-like structure which bears no structural homology to any known fusion protein.[22] However, there are several lines of evidence demonstrating that gH is involved in membrane fusion.[23–26]

Several peptides matching a number of regions of the gH ectodomains have been shown to interact with membranes, and are hypothesized to play a role in the fusion process,[27,28] probably forming a hydrophobic membrane-interacting surface that simultaneously or sequentially could destabilize apposing viral and cellular membranes during fusion. In particular the H^{625}–F^{644} sequence, located in the domain II of gH from herpes simplex virus type I, has been proposed to be actively involved in the process. Indeed, the peptide gH625 corresponding to this sequence has been found to interact with model membranes, folding into an α-helix with amphiphilic characteristics, with most of the hydrophobic residues grouped on the same side.[29] Interaction with this peptide effectively promotes fusion of CHOL-enriched membranes.[30] This is not completely surprising, considering that the gH625 sequence includes the cholesterol recognition/interaction amino acid consensus (CRAC) motif –L/V–$(X)_{(1-5)}$–Y–$(X)_{(1-5)}$–R/K–, in which $(X)_{(1-5)}$ represents between one to five residues of any amino acid.[31–33] However, to date, the actual role played by CHOL in the fusion event is still elusive.

In this scenario, the present work focuses on the interaction of gH625 with lipid bilayers formed by the mixture palmitoyl oleoyl phosphatidylcholine (POPC)–sphingomyelin (SM)–cholesterol (CHOL) (1 : 1 : 1 w/w/w). SM presents the same lipophilic portion of the various sphingolipids naturally occurring in biomembranes. The POPC–SM–CHOL mixture, at the composition used, forms homogeneous bilayers in the liquid-ordered state (L_o),[34] mimicking the lipid raft organization. In order to analyze the role played by each lipid in the peptide–membrane interaction, we also consider bilayers formed by POPC, POPC–SM (2 : 1 w/w) and POPC–CHOL (2 : 1 w/w). POPC and POPC–SM membranes are in the liquid-disordered state (L_α), while POPC–CHOL bilayers, at the composition considered, are in the L_o state.[34] The comparative analysis of the liposome fusion assays, Dynamic Light Scattering (DLS), spectrofluorimetry, Neutron Reflectivity (NR) and Electron Spin Resonance (ESR) experiments, and Molecular Dynamics (MD) simulations is aimed to highlight the specific role of cholesterol and sphingolipids in modulating the peptide–membrane interactions and the resulting peptide fusion ability.

2 Materials and methods

2.1 Materials

Phospholipid palmitoyl oleoyl phosphatidylcholine (POPC), the fluorescent probes *N*-(7-nitro-benz-2-oxa-1,3-diazol-4-yl)phosphatidylethanolamine (NBD-PE) and *N*-(lissamine-rhodamine-B-sulfonyl)phosphatidylethanolamine (Rho-PE) as well as the spin-labeled phosphatidylcholines (1-palmitoyl-2-stearoyl-(*n*-doxyl)-*sn*-glycero-3-phosphocholine, *n*-PCSL, $n = 5, 7, 10, 14$) were obtained from Avanti Polar Lipids (Birmingham, AL, USA). Cholesterol (CHOL), sphingomyelin from chicken egg yolk (SM) and Triton-X100 were obtained from Sigma (St. Louis, MO, USA).

Ultra-high-quality water (resistivity = 18.2 MΩ cm; Elga) was used in all experiments. D_2O (99.7%) for NR experiments was provided by the Institut Laue-Langevin (ILL) in Grenoble, France. The solid supports for neutron reflection were 8 × 5 × 1 cm^3 silicon single crystals cut to provide a surface along the (111) plane. These were polished by Siltronix (Archamps, F) and cleaned for 15 min in a mixture of 1 : 4 : 5 H_2O_2–H_2SO_4–H_2O at 80–85 °C, followed by ozonolysis. This treatment leaves a natural oxide layer of 7–20 Å thickness and 3–5 Å roughness.

2.2 Peptide synthesis

gH625 (NH_2–HGLASTLTRWAHYNALIRAF–$CONH_2$) was synthesized by the solid-phase method using the Fmoc strategy and subsequently purified as previously reported.[30] The purified peptide was shown to be homogeneous (>98%) by analytical HPLC and was obtained in good yields (30–40%). The peptide was further subjected to electrospray mass spectroscopy to confirm its molecular weight.

2.3 Sample preparation

The peptide–membrane interaction was investigated by a combined experimental strategy, including fluorescence, DLS, NR and ESR experiments. POPC, POPC–SM (2 : 1 w/w, ~2 : 1 mol/mol), POPC–CHOL (2 : 1 w/w, ~1 : 1 mol/mol) and POPC–SM–CHOL (1 : 1 : 1 w/w/w, ~1 : 1 : 2 mol/mol/mol) mixtures were used to prepare lipid membranes; *i.e.* CHOL, whenever present, constituted about 50 mol% of the bilayer lipid composition, thus allowing a reliable comparison between the results obtained for the different lipid systems. The bilayer morphology (*e.g.*, various kinds of liposomes, supported bilayers) was optimized for each experimental technique.[35] For fluorescence measurements Large Unilamellar Vesicles (LUVs) with a mean diameter of ~0.1 mm, eventually containing Rho-PE and NBD-PE in addition to unlabelled lipids, were prepared according to the extrusion method in 5 mM HEPES, 100 mM NaCl, pH 7.4. LUVs were also used for DLS measurements. Multi-Lamellar Vesicles (MLVs) including 1% w/w of spin-labeled phosphatidylcholines, to be used for ESR experiments, were prepared by the lipid thin-film hydration method. The samples containing the peptide were prepared following the

same procedure but, in this case, the lipid films were suspended with a specific amount of gH625 solution in buffer. The peptide–lipid ratio was 0.5 : 1 w/w, corresponding to about 0.1 molar ratio. For selected samples, ESR measurements were also performed on LUVs prepared by the extrusion method. No significant difference was observed with respect to measurements performed on MLVs, as shown in the ESI,† indicating that the liposome morphology has no influence on the peptide–lipid interaction.

For neutron reflectivity experiments, Supported Lipid Bilayers (SLBs) were prepared by vesicle fusion:[35] Small Unilamellar Vesicles (SUVs), 25–35 nm in diameter, were formed by vortexing and sonicating for 3 × 10 min the MLV suspension. The SUV suspension (0.5 mg mL^{-1}) was injected into the NR cell, allowed to diffuse and adsorb to the silicon surfaces over a period of 30 min. Afterwards, the sample cell was rinsed once with deuterated water to remove excess lipid. gH625 was added to the bilayer by injecting into the cell an aqueous solution (0.25 mg mL^{-1}) in order to obtain the 0.5 : 1 peptide–lipid weight ratio.

All measurements described below were performed at 310 K.

2.4 Lipid mixing assays

The extent of vesicle fusion was monitored using a Fluorescence Resonance Energy Transfer (FRET) assay to quantify lipid mixing as reported in the literature.[36] Although other methods to measure liposome fusion have been proposed,[37] this remains one of the most widely adopted methods. When two populations of liposomes with different lipid composition fuse, the lipids mix up; consequently, lipids present only in one population are diluted by lipids forming the other population. For the assay adopted in the present work two liposome samples were prepared for each experiment. They presented the same lipid composition with the exception that one of them also included 0.6 mol% of both the labelled lipids NBD-PE (donor) and Rho-PE (acceptor). NBD-PE bears a fluorescent moiety that adsorbs at 465 nm and emits at 530 nm. In the labelled liposomes, NBD-PE emission was effectively quenched by Rho-PE, because of the short spatial distance between them. To start an experiment, labelled vesicles were mixed with unlabelled vesicles in a 1 : 4 ratio (final lipid concentration 0.1 mM). Then, small volumes of peptide in less than 2% v/v dimethylsulfoxide (DMSO) were progressively added and changes in donor emission were monitored. Increased emission revealed an increased distance between NBD-PE and Rho-PE molecules, due to their dilution in the liposomes fused by the peptide action. Thus, the fluorescence intensity was assumed to be proportional to the extent of vesicle fusion. The fluorescence scale was calibrated such that the zero level corresponded to the initial residual fluorescence of the labelled vesicles and the 100% level, corresponding to complete mixing of all lipids in the system, was set by the addition of Triton X-100 (0.05% v/v) at the same total lipid concentrations of the fusion assay.

Each experiment lasted no more than 40 minutes from the mixing of the two liposome populations, thus avoiding possible bias deriving from the transfer of labeled lipids from one liposome to another without fusion.[38] Fluorescence spectra were recorded on a Cary Eclipse spectrofluorimeter (Varian, Palo Alto, CA, USA). A cut-off filter at 515 nm was used between the sample and the emission monochromator to avoid scattering interference.

Lipid mixing experiments were repeated at least three times and the results were averaged.

2.5 Inner-monolayer phospholipid-mixing measurement

The lipid mixing assay does not discriminate between hemifusion and complete fusion of the membranes constituting the liposomes. Whenever hemifusion occurs, only lipids forming the outer leaflets of the membranes mix up, while those constituting the inner leaflets remain separated, delimiting two juxtaposed aqueous pools. Peptide-induced phospholipid-mixing of the inner monolayer was measured by a modification of the phospholipid-mixing measurement as reported elsewhere.[39] Briefly, labelled vesicles were treated with sodium dithionite to completely reduce the NBD located on the outer monolayer of the membrane. The final concentration of sodium dithionite was 100 mM (from a stock solution of 1 M dithionite in 1 M TRIS, pH 10.0) and it was incubated for approximately 30–45 min on ice in the dark. Sodium dithionite was then removed by size exclusion chromatography through a Sephadex G-75 filtration column (Pharmacia, Uppsala, Sweden) eluted with buffer containing 10 mM TRIS, 100 mM NaCl, and 1 mM EDTA, pH 7.4. By this treatment, liposomes labelled only in the inner lipid leaflet were obtained. Fusion of the labelled inner leaflets with unlabelled ones was monitored by following the same protocol described above for lipid mixing assays. Experiments lasted no more than 40 minutes from removal of sodium dithionite, thus avoiding any bias due to translocation (flip-flop) of labelled lipids from the inner to the outer leaflet of the membrane.[38] All experiments were repeated at least three times and the results were averaged.

2.6 Leakage assays

The ANTS/DPX assay was used to measure the ability of the peptide to induce leakage of ANTS/DPX pre-encapsulated in liposomes. This experiment was performed to verify that the lipid bilayer integrity was preserved during the fusion process. Details of this assay can be found elsewhere.[40] To initiate a leakage experiment, the peptide, in a stock solution at pH 7.4 containing 5 mM HEPES and 100 mM NaCl, was added to the stirred vesicle suspension (0.1 mM lipid).

2.7 Dynamic light scattering measurements

DLS measurements were performed with a home-made instrument, as described in the literature.[41] All the solvents used in sample preparation were filtered through a 0.2 μm filter. Considering that the solutions are quite dilute, the Stokes–Einstein equation, which rigorously holds at infinite dilution for non-interacting spherical species diffusing in a continuous medium, was used to evaluate the hydro-dynamic radius R_H of the aggregates from their translational diffusion coefficients D.

2.8 Tryptophan fluorescence measurements

The degree of gH625 association with lipid bilayers was measured by performing spectrofluorimetric titrations of gH625.[30] Small amounts of LUV suspension were progressively added to 4 μM peptide and the fluorescence spectra were recorded between 300 and 400 nm with an excitation wavelength of 295 nm. The fluorescence values were corrected by taking into account the dilution factor corresponding to the addition of microliter amounts of liposome suspension and by subtracting the corresponding blank. The peptide concentration was low enough to cause minimal aggregation in the aqueous phase.

The binding of hydrophobic peptides to membranes can be described as a partition equilibrium,[30] $X_b = K_p C_f$, where K_p is the apparent partition coefficient in units of M^{-1}, X_b is the molar ratio of bound peptide per total lipid and C_f is the equilibrium concentration of the free peptide in solution. Briefly, in this work F_∞, the fluorescence intensity obtained when all the peptide is lipid-bound, was estimated by extrapolation of a double reciprocal plot of the total peptide fluorescence *vs.* the lipid concentration in the outer leaflet, assumed to be 60% of the total lipid concentration. Knowing the fluorescence intensities of the free and bound forms of the peptide, the fraction of the membrane-bound peptide, f_b, could be determined as $f_b = (F - F_0)/(F_\infty - F_0)$, where F represents the fluorescence of the peptide after each addition of the vesicles and F_0 represents the fluorescence of the unbound peptide. The value of f_b allowed to calculate the equilibrium concentration of the free peptide in the solution, C_f, as well as the extent of peptide binding X_b. It was assumed that the peptide was initially partitioned only over the outer leaflet of the LUVs. Therefore, the values of X_b were corrected as $X_b^* = X_b/0.6$.

The curve resulting from plotting X_b^* *versus* the concentration of the free peptide, C_f, is referred to as the conventional binding peptide isotherm. The surface partition coefficients, K_p, was estimated from the initial slope of the curve.

2.9 Neutron reflectivity measurements

NR measurements were performed on the D17 reflectometer at the high flux reactor of the Institut Laue-Langevin (ILL, Grenoble, France) in time-of-flight mode using a range of wavelengths between 2 and 20 Å with two incoming angles of 0.8 and 3.2°.

In a neutron reflectivity experiment, the specular reflection at the silicon/water interface, $R(q)$, is measured as a function of the wave vector transfer, q:

$$q = \frac{4\pi}{\lambda}\sin\theta \quad (1)$$

where λ is the wavelength and θ the angle of the incoming beam to the surface. $R(q)$ is related to the scattering length density across the interface, $\rho(z)$, by:

$$R(q) = \frac{16\pi^2}{q^2}|\hat{\rho}(q)|^2 \quad (2)$$

where $\hat{\rho}(q)$ is the one-dimensional Fourier transform of $\rho(z)$:

$$\hat{\rho}(q) = \int_{-\infty}^{+\infty} \exp(-iqz)\rho(z)\,dz \quad (3)$$

$\rho(z)$ being a function of the distance perpendicular to the interface. ρ is related to the composition of the adsorbed species by:

$$\rho(z) = \sum_j n_j(z) b_j \quad (4)$$

where $n_j(z)$ is the number of nuclei per unit volume and b_j is the scattering length of nucleus j. The scattering lengths of the constituent fragments of any species adsorbed at the surface are the fundamental quantities from which the interfacial properties and microstructural information on the lipid bilayer are derived. Measurement of a sample in different solvent contrasts greatly enhances the sensitivity of the technique.[42]

Samples were measured at 25 °C using H_2O, SMW (silicon-matched water), and D_2O as solvent contrasts. SMW ($\rho = 2.07 \times 10^{-6}$ Å^{-2}) is a mixture of 38 vol% D_2O ($\rho = 6.35 \times 10^{-6}$ Å^{-2}) and 62 vol% H_2O ($\rho = -0.56 \times 10^{-6}$ Å^{-2}) with the same refraction index for neutrons as bulk silicon.

NR profiles were analyzed by box model fitting using initially the AFIT program.[43] It allows the simultaneous analysis of reflectivity profiles from the same sample in different water contrasts, characterizing each layer by its thickness, ρ, solvent volume fraction, and interfacial roughness. These initial model fits were then used as templates for simultaneous fitting of the experimental data using the MOTOFIT program.[44] All the parameters are varied until the optimum fit to the data is found. Although more than one model can be found for a given experimental curve, the number of possible models is greatly reduced by a prior knowledge of the system, which allows defining upper and lower limits of the parameters to be optimized, by the elimination of the physically meaningless parameters, and most importantly by the use of different isotopic contrasts.[42] Initially, the bare silicon substrate was characterized in terms of thickness and roughness. The set of NR profiles were calculated for a uniform single layer model (the silicon oxide layer) of thickness 8 ± 1 Å, roughness 3 ± 1 Å (8 ± 1 Å in one case), and a scattering length density of 3.41×10^{-6} Å^{-2}, corresponding to 100% SiO_2. This step was followed by the characterization of the lipid bilayer and finally of the peptide-interacting bilayer.

2.10 Electron spin resonance spectroscopy

ESR spectra of lipid and lipid–peptide samples were recorded on a 9 GHz Bruker Elexsys E500 spectrometer (Bruker, Rheinstetten, Germany) equipped with a super-high sensitivity probehead. Flame-sealed glass capillaries containing the samples were placed in a standard 4 mm quartz ESR-sample tube containing light silicone oil for thermal stability. The temperature of the sample was regulated and maintained constant during the measurement by blowing thermostated nitrogen gas through a quartz dewar. The instrumental settings were as follows: sweep width, 120 G; resolution, 1024 points;

modulation frequency, 100 kHz; modulation amplitude, 1.0 G; time constant, 20.5 ms, and incident power, 5.0 mW. Several scans, typically 16, were accumulated to improve the signal-to-noise ratio. A quantitative analysis of *n*-PCSL spectra for all lipid samples was realized determining the acyl chain order parameters relative to the bilayer normal, *S*, and the isotropic hyperfine coupling constants for the spin-labels in the membrane, a'_N, through a home-made MATLAB-based software routine, as described in the literature.[45]

2.11 Molecular dynamics simulations

MD simulations have been performed using the NAMD program[46] and the gH625 fragment of the NMR structure in micelle as the starting model.[29] This structure was first immersed in a box containing a POPC–SM–CHOL (1 : 1 : 1 w/w/w, raft-like) bilayer and water molecules. The starting model was placed in the bilayer as suggested in a previous study,[29] *i.e.* forming stabilized electrostatic and hydrophobic interactions with the lipid chains. In particular, Arg633 and Arg642 side chains were located at the bilayer depth of the P lipid atoms, whereas the Trp634 side chain faced towards the bilayer core. The resulting structure presents the inertia principal component of the peptide perpendicular to the bilayer normal. All the solvent molecules with at least one atom within 2 Å from a non-hydrogen atom of the protein were removed. The process of model insertion was performed retaining the POPC–SM–CHOL 1 : 1 : 1 w/w/w composition of the bilayer. Incorporation of the peptide into the bilayer did not induce significant alterations of the system. In order to have an ionic strength of 0.1 M, NaCl was added. Models of each system were generated by using the CHARMM force-field parameters.[47,48] The TIP3P water model was used.[48]

The system was submitted to a minimization procedure of 1000 steps. After this procedure, 2 ns of MD simulations were carried out in the NPT ensemble with a target pressure and temperature equal to 1.013 bar and 310 K, respectively. In this stage a harmonic constraint was used for all protein atoms; 2 fs time-step was used to integrate the Verlet equation. Then, the velocities were reassigned in a semi-isotropic NPT assemble. A total of 300 ns were simulated. 250 ns of equilibrated trajectory have been analyzed. The lipid cross-sectional area on the *x*–*y* plane has not been fixed. This equilibration protocol has been already used in other studies.[49]

The simulation was conducted using a cutoff of 9 Å, a smooth switching function of 7.5 Å and a non-bonded pair list set of 10.5 Å. Long-range electrostatic interactions were computed using the particle-mesh Ewald method with the grid spacing of 1 Å.[50]

3 Results and discussion

3.1 Membrane interaction studies

We first investigated the ability of gH625 to induce fusion between vesicles of POPC or POPC–SM–CHOL (raft-like). A population of vesicles labeled with both NBD- and Rho-labeled PE, used as the donor and acceptor of fluorescence energy transfer, respectively, was mixed with a population of unlabeled LUVs and increasing amounts of peptide were added. The dependence of the extent of lipid mixing on the peptide–lipid molar ratio was analyzed (Fig. 1A).

In the case of membrane fusion induced by the peptide, dilution of labeled lipids should result in a reduction of the fluorescence energy transfer efficiency, hence dequenching (increase) of the donor fluorescence. The graph shows that gH625 effectively fuses POPC–SM–CHOL membranes, while under these experimental conditions we were unable to find any significant activity in POPC vesicles. To investigate the role played by each lipid component, we also considered POPC–CHOL and POPC–SM liposomes. Fig. 1A shows that gH625 presents a fusogenic activity on POPC–CHOL bilayers almost equal to that observed for POPC–SM–CHOL liposomes. No effect was observed on POPC–SM vesicles. Thus, the fusogenic activity of this peptide seems specifically directed towards CHOL-enriched membranes.

The ability of peptides to induce lipid mixing of the inner monolayer, in order to discriminate between hemifusion and complete fusion of the membranes, was also analyzed. In the

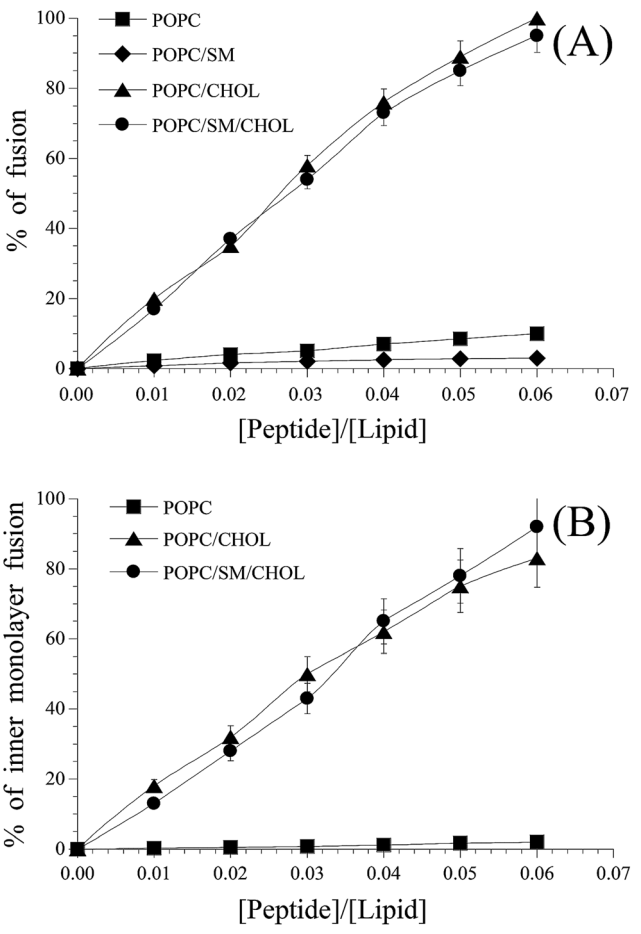

Fig. 1 gH625-promoted membrane fusion of POPC (■), POPC–SM (◆), POPC–CHOL (▲) and POPC–SM–CHOL (1 : 1 : 1 by weight) (●) liposomes as determined by lipid mixing assay (A). gH625-promoted membrane fusion of the inner monolayer of POPC (■), POPC–CHOL (▲) and POPC–SM–CHOL (●) liposomes as determined by lipid mixing assay (B).

inner monolayer assay, the fluorescence from the outer leaflet of the vesicle labeled with NBD- and Rho-PE is eliminated by the addition of an aqueous reducing agent, and this experiment reveals the extent of lipid mixing between the inner monolayers of vesicles in solution. Fig. 1B shows a significant fusion of the inner monolayer in both POPC–SM–CHOL and POPC–CHOL liposomes. This is only slightly lower than the fusion level obtained in the lipid mixing experiment. Therefore, this assay clearly indicates that the peptide is able to induce fusion of both the inner and the outer leaflets constituting the membranes of the liposomes.

Fusion between liposomes reflects in their dimension, as revealed by the DLS measurements reported in the ESI.† In the case of POPC–SM–CHOL LUVs, the average aggregate radius increases from about 100 to 180 nm in the presence of gH625 at a 0.1 peptide/lipid ratio. No variation is detected in the case of POPC liposomes.

The ability of the peptide to induce membrane leakage of POPC–SM–CHOL was also determined, to investigate whether the membrane integrity is preserved during the fusion event. In particular, the release of ANTS and DPX from vesicles is commonly used as a measure of bilayer perturbation and interpreted as "transient pore formation".[40,51] Content-mixing is manifested by a decrease in fluorescence intensity if vesicles encapsulating fluorescent cargo (*e.g.*, ANTS) merge contents with those containing quenchers (*e.g.*, DPX). The leakage experiment, reported in the ESI,† shows that the probe did not leak out significantly to the medium after the interaction with the peptide used in this study.

To evaluate the degree of peptide binding to the membrane bilayers, we measured the intrinsic fluorescence of gH625 in suspensions of liposomes with different compositions (POPC, POPC–CHOL or POPC–SM–CHOL). In all experiments, the increased emission indicated that the single tryptophan residue of the peptide is located in a less polar environment upon interaction with lipids (see the ESI† for an example). The increase in fluorescence for tryptophan binding to membrane phospholipids was used for the generation of binding isotherms, also reported in the ESI,† from which partition coefficients were calculated. The results, collected in Table 1, show a stronger tendency of gH625 to interact with POPC–CHOL or POPC–SM–CHOL bilayers than with POPC ones. Interestingly, similarly to what observed for the membrane fusion assay, the K_p value obtained for POPC–CHOL coincides, within the experimental uncertainty, with that obtained for POPC–SM–CHOL. This indicates that the peptide–bilayer association is fundamentally tuned by the CHOL present in the membrane.

Table 1 Partition coefficients of gH625 in lipid bilayers

	$K_p \times 10^{-3}/M^{-1}$
POPC	2.5 ± 0.2
POPC–CHOL	18 ± 2
POPC–SM–CHOL	21 ± 2

3.2 NR data

First, POPC and POPC–SM–CHOL bilayers in the absence of gH625 peptide were characterized by using D_2O, SMW and H_2O as isotopic contrast solvents. The experimental curves are shown in Fig. 2A and C and the parameters used to fit the curves simultaneously from all the contrasts are given in Table 2. A schematic representation of the results is reported in Fig. 3. For both systems, a five box model was found to best fit the data. The first two boxes correspond to the silicon oxide and to the thin solvent layer interposed between the silicon surface and the adsorbed bilayer. The three other boxes describe the lipid bilayer, which is subdivided into the inner headgroup, the hydrophobic chain, and the outer headgroup layers. The theoretical scattering length density, ρ, was calculated through eqn (4).

In the case of POPC, the ρ of the lipid headgroups is equal to 1.86×10^{-6} Å^{-2}, while the ρ of the acyl chains is equal to -0.29×10^{-6} Å^{-2}.[35,52] These values were kept constant during the data analysis, since their optimization was found to give no fitting improvement. Thus, the parameters obtained from the best-fit procedure are the thickness and the roughness of each box plus the solvent content expressed as volume percent. Inspection of Table 2 indicates that the overall thickness of the bilayer is 43 ± 1 Å and the solvent content is (35 ± 10)% for both headgroup layers. In the case of the bilayers also containing SM and CHOL, a total thickness of 48 ± 1 Å and a solvent content in the headgroup region of (∼22 ± 10)% for the inner and outer polar layers were obtained by the fitting model. ρ is equal to $\sim -0.1 \times 10^{-6}$ Å^{-2} for the acyl chain region, confirming the presence of cholesterol in this part of the bilayer, while the ρ value for the headgroup region is equal to 1.7×10^{-6} Å^{-2}. For both considered bilayers, any model without a water layer between the substrate and the bilayer gave a bad fit to the data. These NR results are in agreement with those previously reported[35,52] and show that POPC–SM–CHOL bilayers are thicker and substantially less hydrated with respect to POPC ones.

The effect of gH625 on the bilayers was studied by measuring the neutron reflectivity curves of the pure POPC and POPC–SM–CHOL membranes to which the peptide was added. NR curves are shown in Fig. 2B and D. The values of all parameters optimized in curve fitting are reported in Table 2. In Fig. 3, a schematic representation of changes in lipid bilayers due to the presence of the gH625 peptide is shown.

Data from the POPC bilayer interacting with the peptide were fitted by an additional layer with respect to the case of the pure lipid model. The model suggests that the peptide prominently interacts with the outer bilayer surface; the peptide ρ was calculated from eqn (4) and is equal to 1.9×10^{-6} Å^{-2}. In order to obtain a good curve fitting, it was not necessary to change the ρ values of all lipid membrane layers, thus suggesting that their composition remains unchanged, *i.e.* no peptide penetration. Inspection of Table 2 reveals, as only effect of the peptide, that the thickness of the outer hydrophilic layer decreases by ∼3 Å, indicating that gH625 interacts with the membrane surface, perturbing only the external region. NR profiles corresponding to the POPC–SM–CHOL bilayer in the presence of gH625 were also analyzed. In this case, a good curve fitting was obtained

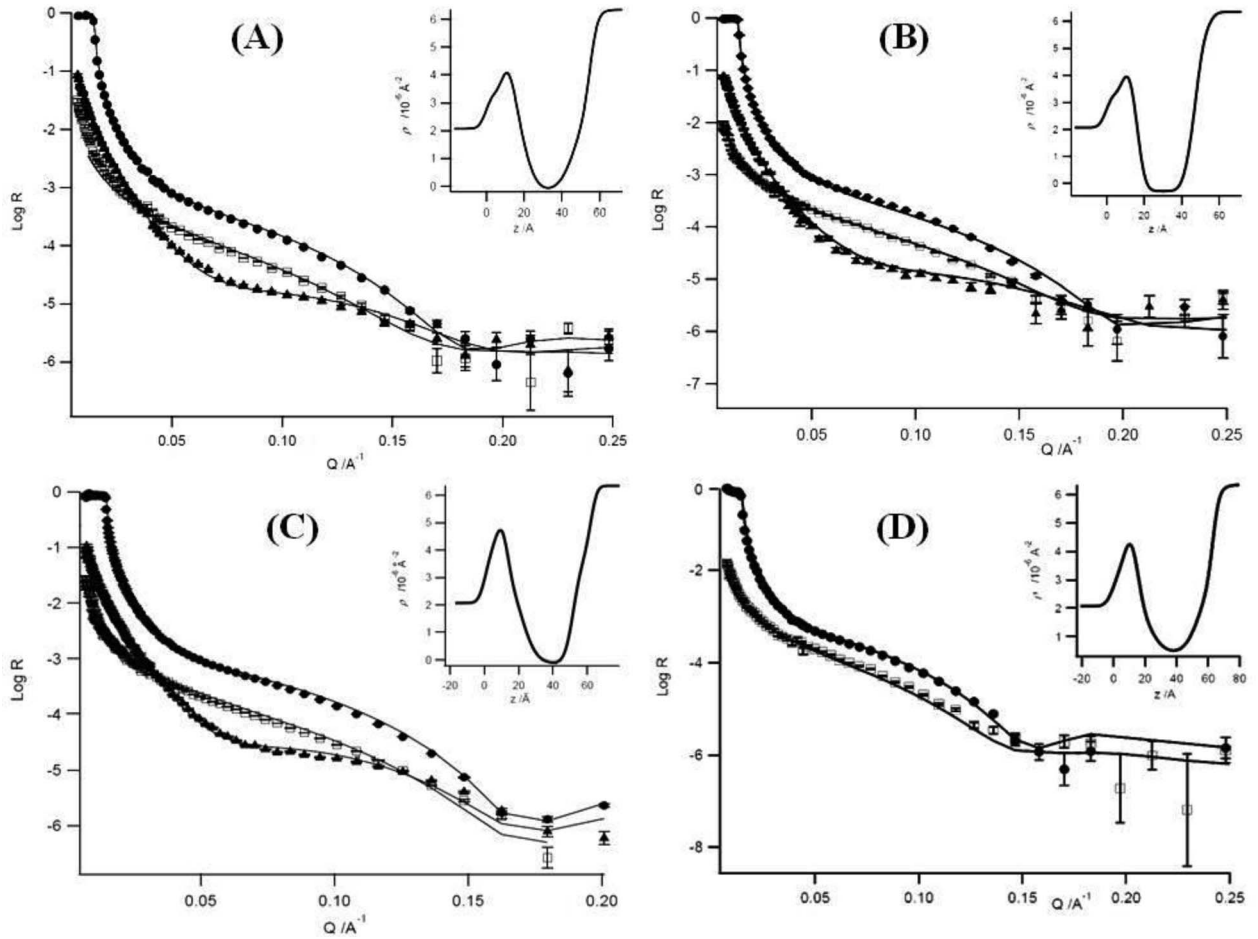

Fig. 2 NR profiles (points) and best fits (continuous lines) corresponding to POPC bilayers in the absence (A) and presence (B) of hydrogenated gH625; POPC–SM–CHOL bilayers in the absence (C) and presence (D) of hydrogenated gH625 peptide. D_2O (●), SMW (□) and H_2O (▲) were used as contrast solvents. The insets show the ρ profiles for the lipid bilayers in D_2O.

Table 2 Values (±standard deviations) of the parameters derived from model fitting of the reflectivity profiles for lipid bilayers in the absence and in the presence of gH625

	Interfacial layer	Thickness (Å)	% Solvent	Roughness (Å)
POPC	Water	3 ± 1	100	3 ± 1
	Inner headgroups	7 ± 1	35 ± 10	5 ± 1
	Chain region	29 ± 2	—	6 ± 2
	Outer headgroup	7 ± 1	35 ± 10	7 ± 1
+gH625	Water	3 ± 1	100	3 ± 1
	Inner headgroups	5 ± 1	34 ± 10	5 ± 1
	Chain region	28 ± 2	—	3 ± 2
	Outer headgroup	4 ± 1	35 ± 10	4 ± 1
	Interacting peptide	6 ± 1	84 ± 10	3 ± 1
POPC–SM–CHOL	Water	5 ± 1	100	4 ± 1
	Inner headgroups	7 ± 1	23 ± 10	4 ± 1
	Chain region	34 ± 2	—	5 ± 2
	Outer headgroup	7 ± 1	22 ± 10	7 ± 1
+gH625	Water	5 ± 1	100	4 ± 1
	Inner headgroups	5 ± 1	32 ± 10	4 ± 1
	Chain region	37 ± 2	—	9 ± 2
	Outer headgroup	10 ± 1	40 ± 10	8 ± 1

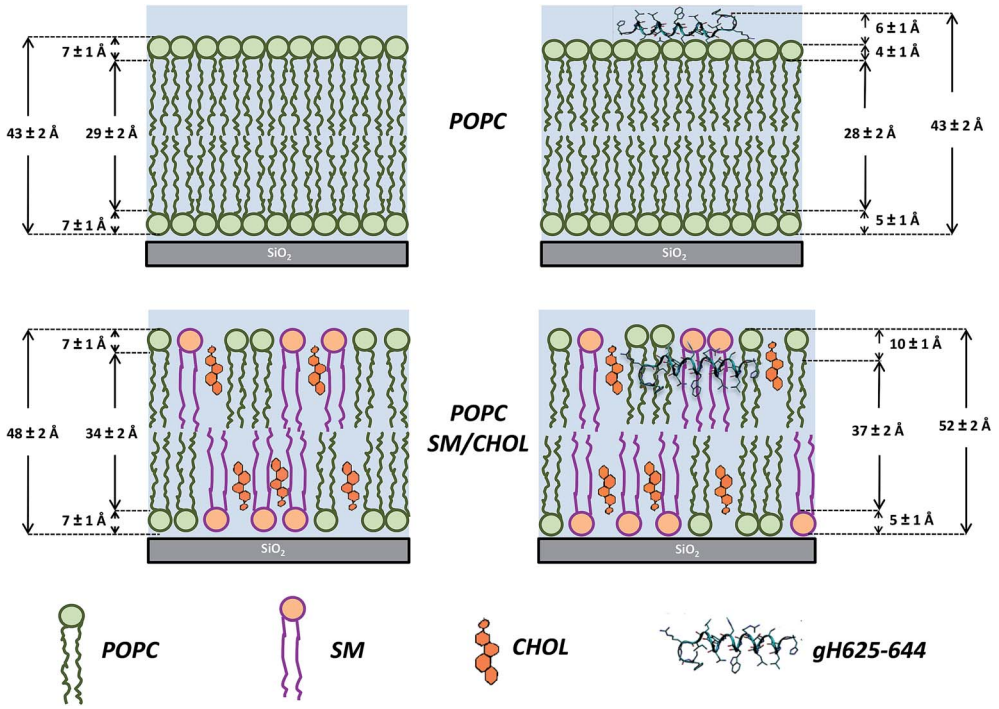

Fig. 3 Schematic representation of lipid bilayers at different lipid concentrations in the absence and presence of the gH625 peptide, with indication of some structural parameters obtained by NR measurements. The image of the peptide is only to indicate the location of gH625 in the bilayer, the orientation being not implied from NR data.

without the additional layer, but varying all parameters related to the hydrophobic and hydrophilic layers. In particular, ρ changes were observed for the hydrophobic region and the outer headgroup region. In the first case, ρ increases to a value of $\sim 0.36 \times 10^{-6}$ Å^{-2}, while for the hydrophilic layer it becomes equal to $\sim 1.9 \times 10^{-6}$ Å^{-2}. This evidence indicates that the peptide strongly interacts with the lipid membranes, partially penetrating into the hydrophobic core. In addition, for both hydrophobic and outer hydrophilic regions the thickness increases by ~ 3 Å, confirming the peptide insertion, while roughness values undergo only a slight variation. The gH625 addition also causes an increase of the solvent content in the external headgroup layer, while no changes in the solvent content for the acyl chain region was observed. Finally, for the inner hydrophilic layer a small decrease of the thickness and an increase of the roughness was detected, indicating that it was slightly but significantly perturbed although the gH625 peptide does not interact with it.

3.3 ESR data

The membrane–peptide interaction was also investigated by ESR measurements, incorporating phosphatidylcholines spin-labeled on the different positions of the *sn*-2 chain (*n*-PCSL, with $n = 5, 7, 10, 14$) in the lipid bilayers; 5-PCSL monitors the bilayer region just underneath the hydrophilic interface, while in the case of 14-PCSL the reporter group is deeply embedded in the inner hydrophobic core. *n*-PCSL spectra in POPC and POPC–SM–CHOL membranes in the absence and presence of gH625 are shown in Fig. 4 and 5.

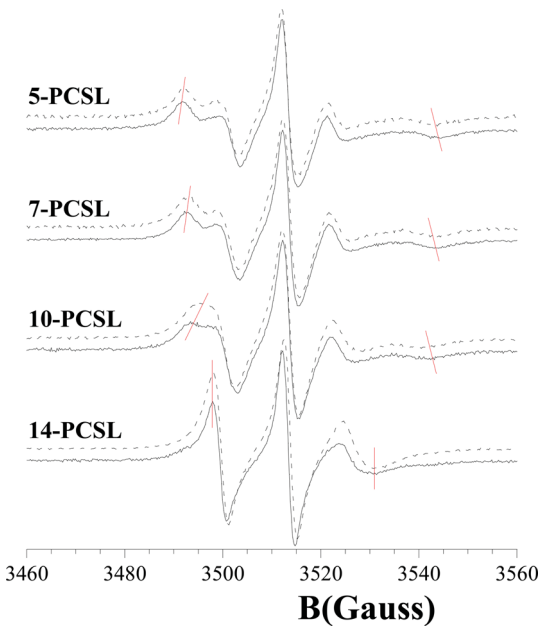

Fig. 4 ESR spectra of *n*-PCSL in POPC bilayers in the absence (solid line) of peptide and in the presence (dotted line) of gH625. Red segments are guides to the eye highlighting shifts of maximum and minimum points.

We first analyze the spectra registered without the peptide (solid lines in the figures). In both lipid systems, 5-PCSL shows a clearly defined axially anisotropic behavior, as detectable by the

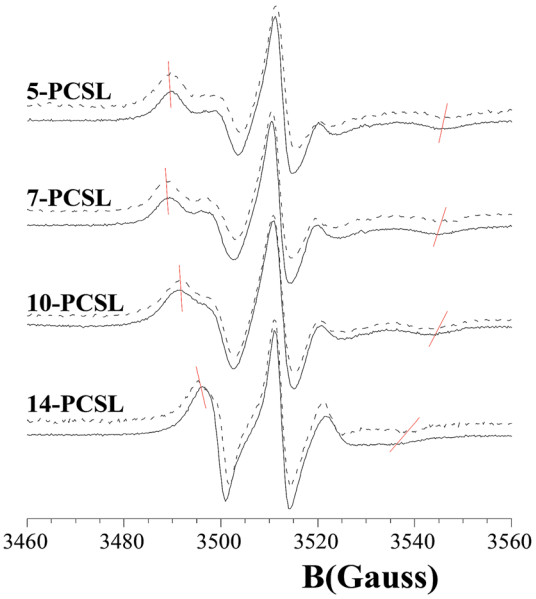

Fig. 5 ESR spectra of *n*-PCSL in POPC–SM–CHOL bilayers in the absence (solid line) of peptide and in the presence (dotted line) of gH625. Red segments are guides to the eye highlighting shifts of maximum and minimum points.

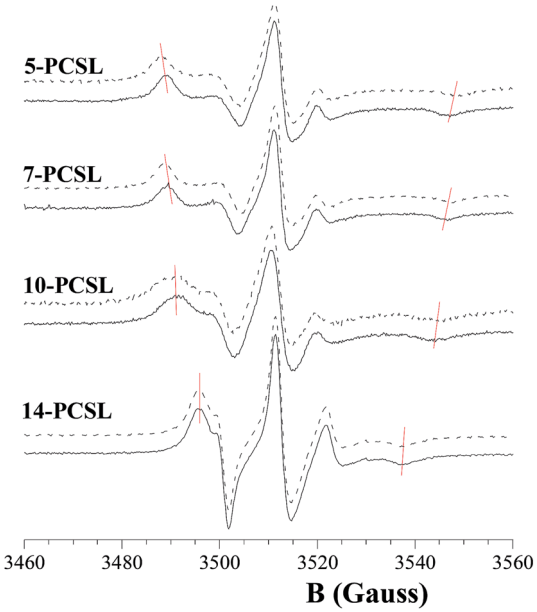

Fig. 6 ESR spectra of *n*-PCSL in POPC–CHOL bilayers in the absence (solid line) of peptide and in the presence (dotted line) of gH625. Red segments are guides to the eye highlighting shifts of maximum and minimum points.

splitting of the low- and high-field lines, indicating an ordered organization of the outer segments of the lipid acyl chains.

As the reporter group is stepped down along the acyl chain, a different behavior is observed for the two lipid systems: in POPC bilayers the spectrum anisotropy markedly decreases and, in the case of 14-PCSL, a three-line quasi-isotropic spectrum is obtained. In contrast, in POPC–SM–CHOL bilayers the spectrum anisotropy is preserved for all the spin-labels. This evidence unequivocally indicates that POPC membranes are in the liquid-disordered (L_α) crystalline state, while the POPC–SM–CHOL ones are in the liquid-ordered (L_o) state.[53]

For both lipid systems, the addition of gH625 causes significant variations in the *n*-PCSL's spectra, although in the opposite direction, see Fig. 4 and 5 (dotted lines). In the case of POPC membranes, a decrease of the anisotropic behavior is observed, as highlighted by the decreased distance (in Gauss) between the high-field maximum and the low-field minimum. The opposite is observed for POPC–SM–CHOL bilayers.

We also considered POPC–CHOL bilayers, see the spectra in Fig. 6. POPC–CHOL membranes, at the composition considered in this work, are in the L_o state, as detectable by the similarity of their ESR spectra with those obtained for the POPC–SM–CHOL bilayers. However, interesting differences arise when the spectra registered in the presence of gH625 are considered. Indeed, while in the case of POPC–SM–CHOL bilayers the perturbations due to the peptide are evident at all spin-label positions, in the case of POPC–CHOL membranes the spectra of the inner spin-labels seem to be less affected than those bearing the reporter group close to the bilayer interface.

A quantitative analysis of *n*-PCSL spectra was realized determining the order parameter, S, and the hyperfine coupling constant, a'_N. S is a measure of the local orientational ordering of the labeled molecule with respect to the normal to the bilayer surface, while a'_N is an index of the micropolarity experienced by the nitroxide. Fig. 7 shows the dependence of S on the chain position, n, for the *n*-PCSL spin-labels in lipid membranes, with and without gH625 peptide, while the a'_N values are reported in Table 3.

In the case of POPC membranes, the addition of peptide causes a decrease of the S value to the same extent (~0.4) for 5, 7 and 10-PCSL. For the 14-PCSL spectrum, no S change is observed. This is evidence that the peptide binds solely at the membrane surface, causing a major fluidity of the bilayer, and does not penetrate appreciably into the membrane interior.

In contrast, the addition of the gH625 peptide to the POPC–SM–CHOL membranes causes an increase of S values for all spin-labels. In particular, it increases at 5, 7 and 10 chain positions to the same extent (~0.3). For the 14-PCSL, a more significant change was observed in the ESR spectrum, which presents an evident anisotropic lineshape and an S increase from 0.35 to 0.45. This is evidence that the peptide partially penetrates into the bilayer interior, reducing the mobility of the lipid acyl chains. No change in the a'_N values upon peptide addition to the bilayer was observed, see Table 3. This parameter is related to the polarity of the local environment in which the reporter group is embedded. Consequently, this evidence indicates that gH625 penetrating POPC–SM–CHOL membranes does not carry hydration water molecules, consistent with NR results previously discussed.

For POPC–CHOL bilayers an S increase is observed in the presence of gH625, similarly to what observed for POPC–SM–CHOL. However, the difference decreases with increasing n, indicating that the inner core of the bilayer is less affected by the peptide interaction.

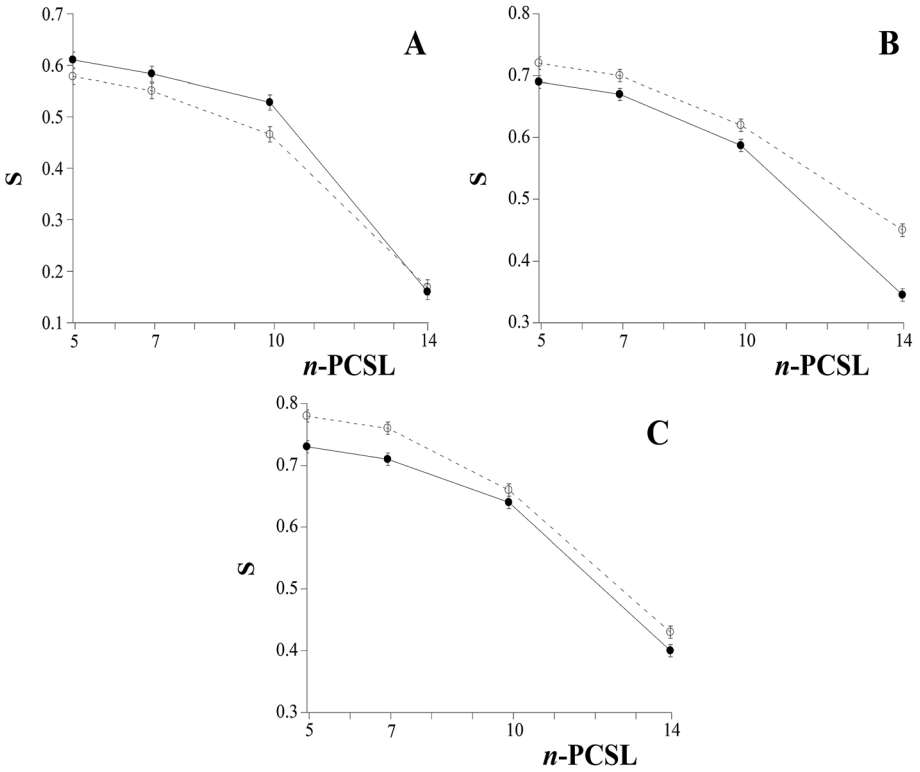

Fig. 7 Dependence on spin-label position, *n*, of the order parameter, *S*, of the *n*-PCSL phosphatidylcholine spin labels in membranes of POPC (A), of POPC–SM–CHOL (B) and POPC–CHOL (C), in the absence (●, continuous line) and presence of gH625 (○, dotted line) peptide.

3.4 MD results

In order to examine at the atomic level the interactions between gH625 and the components of the POPC–SM–CHOL bilayer, a 300 ns long MD simulation has also been performed. First, we have analyzed the conformation adopted by the peptide and have tried to identify the positioning of each part of the peptide during the simulation, calculating the probability to find each residue at a given *Z*-axis value of the bilayer (data not shown). It is found that the peptide retains its starting amphiphilic α-helical structure and remains mostly embedded among the lipid headgroups, with the helix axis almost parallel to the bilayer surface. Cα atoms are located between the P and carbonilic O lipid atoms, but closer to the second. Some side chains of the peptide are oriented towards the lipid core and others towards the exterior of the lipid bilayer. In particular, His625, Leu627, Leu631, Trp634, Asn638, Ile641 and Phe644 present their side chains facing towards the interior of the lipid bilayer, while Ser629, Thr632, Arg633, His636, Leu640 and Arg642 (Fig. 8) have their side chains towards the hydrophilic region.

To identify in more detail the positioning of Arg633, Trp634 and Arg642 side chains, the *Z*-axis position of the gH625 Cα mass center and side chain atoms of these residues when compared to that occupied on average by the P lipid atoms (Δr) has been calculated and reported in Fig. 9 as a function of time. It is found that Arg side chains are exposed to the solvent, whereas the Trp634 side chain protrudes towards the lipid core at a depth of about 9 Å from the lipid P atoms. This finding supports the results already reported analyzing the Trp634 fluorescence spectrum in POPC–CHOL vesicles.[30] The Trp

Table 3 a'_N values of *n*-PCSL in liposomes of pure POPC, POPC–SM–CHOL and POPC–CHOL in the absence and presence of the gH625 peptide

	a'_N/G					
n-PCSL	POPC	POPC + gH625-644	POPC–SM–CHOL	POPC–SM–CHOL + gH625-644	POPC–CHOL	POPC–CHOL + gH625-644
5-PCSL	15.3 ± 0.1	15.2 ± 0.1	15.4 ± 0.1	15.8 ± 0.1	15.3 ± 0.1	15.5 ± 0.1
7-PCSL	15.1 ± 0.1	15.1 ± 0.1	15.4 ± 0.1	15.8 ± 0.1	15.1 ± 0.1	15.4 ± 0.1
10-PCSL	14.9 ± 0.2	14.7 ± 0.2	15.2 ± 0.1	15.2 ± 0.1	14.9 ± 0.1	15.2 ± 0.1
14-PCSL	13.6 ± 0.2	13.9 ± 0.2	14.1 ± 0.2	14.2 ± 0.2	14.1 ± 0.2	14.5 ± 0.2

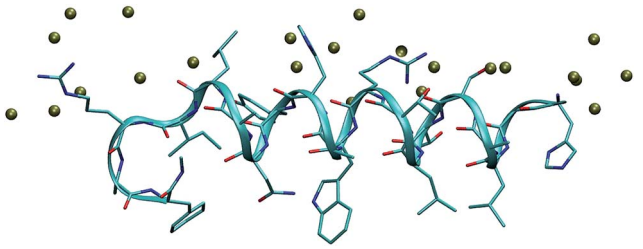

Fig. 8 Structure of the peptide inserted in the bilayer. P lipid atoms are represented as brown spheres.

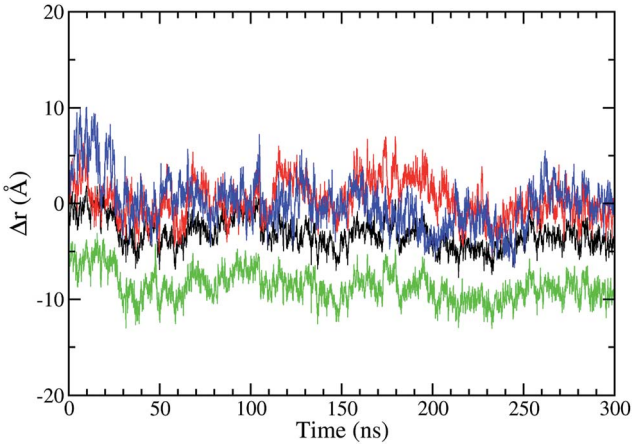

Fig. 9 Z-axis position of the Cα (black) and side chain atoms of the Arg633 (red), Trp634 (green) and Arg642 (blue) when compared to the average value of the P lipid atoms during the MD simulation. A value of Δr equal to 0 Å indicates that the considered atoms are located within the hydrated region of the bilayer, exactly at the same depth of the P lipid atoms; positive values of Δr indicate that the considered atoms are located at the exterior of the lipid bilayer, whereas negative values indicate that they are within the bilayer.

residue interacts principally with one CHOL molecule during the simulation (see for example Fig. 10A). The distances between the O3 atom of this CHOL molecule and the Trp634 Nε1 and Asn638 Oδ1 atoms have been followed as a function of time (Fig. 10B). During the simulation, the NεH atom of the Trp634 side chain forms a hydrogen bond with the OH group of CHOL. This hydrogen bond is assisted by the Asn638 side chain (Fig. 10B). These interactions stabilize the peptide in the bilayer and suggest a role for CHOL molecules in stabilizing the peptide insertion in the lipid core. Interestingly, we did not found any specific interaction of Tyr637 with CHOL or other lipid molecules. This residue belongs to the CRAC motif, and has been speculated to play a pivotal role in recognizing CHOL molecules in the membrane, even though its actual role is still debated.[54]

Special attention was then devoted to N-terminal residue His625, which has been suggested to play an important role in the peptide–bilayer interaction.[30] Notably, although the N-terminal region of the peptide is located at the same depth of P lipid atoms in the bilayer, the side chain of this residue is located at the same bilayer depth as the carbonylic lipid O atoms and is oriented towards the lipid core (Fig. 8). In particular, the integration of the radial pair distribution function shows that there are on average 0.6 carbonylic lipid O atoms at 3.5 Å from the His625 Nδ1 atom. This finding suggests the formation of a rather stable hydrogen bond. This peptide–lipid direct interaction can suggest the mechanism by which the presence of His in this position can help to incorporate the peptide in the bilayer.

The packing of the peptide in the bilayer has also been estimated by evaluating the number of neighbor molecules, where neighbors are defined as objects that have at least one atom in close contact (<4.0 Å) with the peptide. The average number of POPC and SM neighbors of the peptide is 7 and 6 ± 1, respectively, whereas this value has been estimated to be within 3 ± 1 for CHOL.

3.5 Biological implications

Recent studies have demonstrated that the receptor nectin 1, in the presence of the $\alpha_V\beta_3$-integrin, could drive HSV to the lipid rafts of the target cell, where virus entry occurs through a raft-dependent pathway.[18,19] Consequently, it is reasonable to hypothesize that the virus has developed a molecular machinery optimally suited to fuse its own envelope with sterol- and sphingolipid-enriched membranes. In this work, we have demonstrated that the peptide gH625, encompassing one of the membranotropic segments of the gH glycoprotein

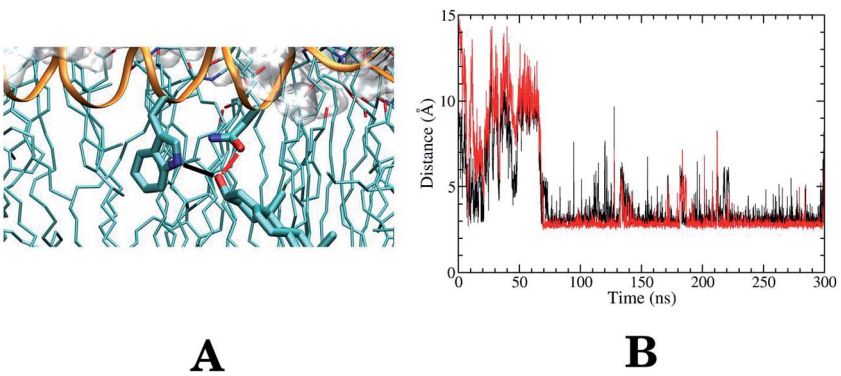

Fig. 10 Hydrogen bond interaction between CHOL and both Trp634 and Asn638 residues (A). Distance *vs.* time of the CHOL O3 atom from the Trp634 Nε1 (black) and Asn638 Oδ1 (red) atoms (B).

of the HSV type I, presents a specific fusogenic activity on CHOL- and SM-containing bilayers in the L_o state, representative of naturally occurring lipid-rafts. In contrast, it is almost inactive on fluid phospholipid membranes in the L_α state. This specificity derives from the different mechanisms of interaction of the peptide with the two kinds of lipid membranes and from the different effects it exerts on the lipid arrangement.

In the case of raft-like bilayers, gH625 partially penetrates into the membrane, positioning between the hydrophilic layer formed by the lipid headgroups and the hydrophobic core formed by the acyl chains. This location is favored by the conformation of the peptide, which adopts an amphiphilic α-helical structure, with polar and charged residues on one side and apolar residues mostly grouped on the opposite side. The helix axis lies almost parallel to the membrane interface with comparable deepness of insertion of N- and C-termini. Most of the hydrophobic residues (Leu627, Leu631, Trp634, Ile641, Phe644) insert their side chains among the lipid acyl chains, while hydrophilic residues (Ser629, Thr632, Arg633) are embedded among the largely hydrated lipid headgroups. The residue more deeply inserted into the bilayer is Trp634 that, forming a hydrogen bond with the CHOL hydroxyl, stabilizes the peptide–membrane interaction. A similar conclusion was drawn for other peptides derived from the fusion glycoproteins gp36 of the Feline Immunodeficiency Virus (FIV)[35] and E1 of the Hepatitis C Virus.[55] This evidence suggests a key role played by tryptophans, for the peptide, and by CHOL for the lipid, in the protein/membrane interplay occurring during viral fusion.

Particularly, our results show that, independent of the presence of SM, CHOL is able to drive the membrane interaction with the membranotropic protein domain. POPC–CHOL and POPC–SM–CHOL bilayers are equally fused by gH625 and the peptide presents the same partition coefficient in these lipid mixtures. For these bilayers, which are in the L_o state, the presence of the peptide causes an increased order of the lipid acyl chains, whose local rotational motion is significantly hampered. The stiffening of the peptide-interacting bilayer leaflet results in an asymmetric perturbation of the membrane, which is locally destabilized thus favoring fusion but not leakage events. Interestingly, the presence of SM seems to tune the effects of the peptide on the lipid ordering and dynamics. While in the case of POPC–CHOL membranes lipid perturbation is limited to the more external portion of the acyl chains, for POPC–SM–CHOL bilayers it propagates along the whole chains.

gH625 also interacts with fluid phospholipid bilayers. However, in this case it tends to localize above the external hydrophilic layer. As an indirect effect of this "adsorption" the lipid chains become even more disordered and their rotational motions increase. These perturbations do not promote the membrane fusion. A possible explanation is that fluid and disordered membrane are able to re-arrange opposing the effect of the peptide, thus neutralizing its destabilizing activity. Thus, ordered and relatively rigid rafts are much more easily led to fuse.

Our findings support the relevance of alterations of lipid dynamics, as recently proposed for other raft-related pathologies.[56,57] The fine tuning of acyl chain order and segmental motion, operated at the microscopic level by interacting proteins, peptides or other guest molecules, reflects in mesoscopic membrane features (*e.g.*, local curvature, permeability, stability), which in turn determine the membrane macroscopic functional behavior. Since in lipid rafts the lipid–lipid and lipid–protein interplay is enhanced, interacting guests cause more effective perturbations.

4 Conclusions

gH625, a membranotropic fragment of the glycoprotein gH of the Herpes Simplex Virus (HSV) type I, drives fusion of L_o raft-like lipid bilayers. The comparative analysis of liposome fusion assays, Dynamic Light Scattering (DLS), spectrofluorimetry, Neutron Reflectivity (NR) and Electron Spin Resonance (ESR) experiments, and Molecular Dynamics (MD) simulations shows that, in the presence of CHOL, gH625 partially penetrates into the membrane, adopting an amphiphilic α-helical structure. The peptide–bilayer association is stabilized by specific Trp–CHOL interactions. gH625 causes an increased order of the lipid acyl chains, whose local rotational motion is significantly hampered. The stiffening of the peptide-interacting bilayer leaflet results in an asymmetric perturbation of the membrane, which is locally destabilized thus favoring fusion events. Altogether, our results clearly indicate the relevance of CHOL as a key player in the membrane fusion process.

The present study, besides furnishing a contribution to the elucidation of the molecular details underlying a complex phenomenon of biological interest, such as viral fusion, gives a scientific support to the exploitation of peptides derived from fusion glycoproteins for drug delivery. In particular, gH625 has been already demonstrated to be able to transport a cargo into the cytoplasm and across the blood–brain barrier.[58] Moreover, the possibility to conjugate gH625 with liposomes, nanoparticles and dendrimers,[58] enhancing their intracellular penetration, has been reported. Our results point to the need of a correct choice of the carrier peptide in relation to composition and features of the membrane of the target cell. In this direction, gH625 is optimally suited for cells whose membrane is enriched in cholesterol and sphingolipids.

Acknowledgements

This work was supported by MIUR (PRIN 2010–2011, Grant 2010NRREPL). GV thanks the Institut Laue-Langevin for awarding beam time.

References

1 K. Simons and J. L. Sampaio, *Cold Spring Harbor Perspect. Biol.*, 2011, **3**, a004697.
2 L. J. Foster, Lipid Rafts, in *Cellular Domains*, ed. I. R. Nabi, John Wiley & Sons, Inc, 1st edn, 2011.

3 N. Gupta and A. L. De Franco, *Semin. Cell Dev. Biol.*, 2007, **18**, 616.
4 K. Gaus, S. Le Lay, N. Balasubramanian and M. A. Schwartz, *J. Cell Biol.*, 2006, **174**, 725.
5 G. van Meer, E. Stelzer, R. Wijnaendts-van-Resandt and K. Simons, *J. Cell Biol.*, 1987, **105**, 1623.
6 D. A. Hicks, N. N. Nalivaeva and A. J. Turner, *Front. Physiol.*, 2012, **3**, 189.
7 S. S. Rawat, M. Viard, S. A. Gallo and A. Rein, *Mol. Membr. Biol.*, 2003, **20**, 243.
8 T. Takahashi and T. Suzuki, *Biochem. Res. Int.*, 2011, 245090.
9 T. Suzuki and Y. Suzuki, *Biol. Pharm. Bull.*, 2006, **29**, 1538.
10 S. C. Harrison, *Nat. Struct. Mol. Biol.*, 2008, **15**, 690.
11 S. Rauch and O. T. Fackler, *Signal Transduction*, 2007, **7**, 53.
12 M. Umashankar, C. Sanchez-San Martin, M. Liao, B. Reilly, A. Guo, G. Taylor and M. Kielian, *J. Virol.*, 2008, **82**, 9245.
13 B. Apellaniz, E. Rujas, P. Caravilla, J. Roquejo-Isidro, N. Huarte, C. Domene and J. L. Nieva, *J. Virol.*, 2014, **88**, 13367.
14 S. Bavari, C. M. Bosio, E. Wiegand, G. Ruthel, A. B. Will, T. W. Geisbert, M. Hevey, C. Schmaljohn, A. Schmaljohn and M. J. Aman, *J. Exp. Med.*, 2002, **195**, 593.
15 M. S. Freitas, C. Follmer, L. T. Costa, C. Vilani, M. L. Bianconi, C. A. Achete and J. L. Silva, *PLoS One*, 2011, **6**, e15756.
16 M. Veit and B. Tha, *Adv. Virol.*, 2011, 370606.
17 J. J. Martín, J. Holguera, L. Sánchez-Felipe, E. Villar and I. Muñoz-Barroso, *Biochim. Biophys. Acta, Biomembr.*, 2012, **1818**, 753.
18 T. Gianni and G. Campadelli-Fiume, *J. Virol.*, 2012, **86**, 2850.
19 T. Gianni, V. Gatta and G. Campadelli-Fiume, *Proc. Natl. Acad. Sci. U. S. A.*, 2010, **107**, 22260.
20 F. C. Bender, J. C. Whitbeck, L. Ponce, H. Lou, R. J. Eisenberg and G. H. Cohen, *J. Virol.*, 2003, **77**, 9542.
21 A. Turner, B. Bruun, T. Minson and H. Browne, *J. Virol.*, 1998, **72**, 873.
22 T. K. Chowdary, T. M. Cairns, D. Atanasiu, G. H. Cohen, R. J. Eisenberg and E. E. Heldwein, *Nat. Struct. Mol. Biol.*, 2010, **17**, 882.
23 A. Farnsworth, T. W. Wisner, M. Webb, R. Roller, G. Cohen, R. Eisenberg and D. C. Johnson, *Proc. Natl. Acad. Sci. U. S. A.*, 2007, **104**, 10187.
24 G. Vitiello, A. Falanga, M. Galdiero, D. Marsh, S. Galdiero and G. D'Errico, *Biochim. Biophys. Acta, Biomembr.*, 2011, **1808**, 2517.
25 T. Gianni, A. Piccoli, C. Bertucci and G. Campadelli-Fiume, *J. Virol.*, 2006, **80**, 2216.
26 R. P. Subramanian and R. J. Geraghty, *Proc. Natl. Acad. Sci. U. S. A.*, 2007, **104**, 2903.
27 S. Galdiero, A. Falanga, M. Vitiello, H. Browne, C. Pedone and M. Galdiero, *J. Biol. Chem.*, 2005, **280**, 28632.
28 S. Galdiero, A. Falanga, G. Vitiello, M. Vitiello, C. Pedone, G. D'Errico and M. Galdiero, *Biochim. Biophys. Acta, Biomembr.*, 2010, **1798**, 579.
29 S. Galdiero, L. Russo, A. Falanga, M. Cantisani, M. Vitiello, R. Fattorusso, G. Malgieri, M. Galdiero and C. Isernia, *Biochemistry*, 2012, **51**, 3121.
30 S. Galdiero, A. Falanga, M. Vitiello, L. Raiola, L. Russo, C. Pedone, C. Isernia and M. Galdiero, *J. Biol. Chem.*, 2010, **285**, 17123.
31 H. Li and V. Papadopoulos, *Endocrinology*, 1998, **139**, 4991.
32 S. A. Vishwanathan, A. Thomas, R. Brasseur, R. F. Epand, E. Hunter and R. M. Epand, *Biochemistry*, 2008, **47**, 11869.
33 C. Schroeder, *Subcell. Biochem.*, 2010, **51**, 77.
34 D. Marsh, *Biochim. Biophys. Acta, Biomembr.*, 2009, **1788**, 2114.
35 G. Vitiello, G. Fragneto, A. A. Petruk, A. Falanga, S. Galdiero, A. M. D'Ursi, A. Merlino and G. D'Errico, *Soft Matter*, 2013, **9**, 6442.
36 D. K. Struck, D. Hoekstra and R. E. Pagano, *Biochemistry*, 1981, **20**, 4093.
37 J. Wilschut and D. Papahadjopoulos, *Nature*, 1979, **281**, 690.
38 M. S. C. Abreu, M. J. Moreno and W. L. C. Vaz, *Biophys. J.*, 2004, **87**, 353.
39 J. E. Cummings and T. K. Vanderlock, *Biochim. Biophys. Acta, Biomembr.*, 2007, **1768**, 1796.
40 R. A. Parente, S. Nir and F. C. Szoka Jr, *Biochemistry*, 1990, **29**, 8720.
41 G. Mangiapia, G. D'Errico, L. Simeone, C. Irace, A. Radulescu, A. Di Pascale, A. Colonna, D. Montesarchio and L. Paduano, *Biomaterials*, 2012, **33**, 3770.
42 G. Fragneto, R. K. Thomas, A. R. Rennie and J. Penfold, *Langmuir*, 1996, **12**, 6036.
43 P. N. Thirtle, *Afit Simulation Program*, Oxford University, Oxford, UK, 1997, vol. 3.1.
44 A. Nelson, *J. Appl. Crystallogr.*, 2006, **39**, 273.
45 G. D'Errico, A. Silipo, G. Mangiapia, G. Vitiello, A. Molinaro, R. Lanzetta and L. Paduano, *Phys. Chem. Chem. Phys.*, 2010, **12**, 13574.
46 J. C. Phillips, R. Braun, W. Wang, J. Gumbart, E. Tajkhorshid, E. Villa, C. Chipot, R. D. Skeel, L. Kale and K. Schulten, *J. Comput. Chem.*, 2005, **26**, 1781.
47 J. B. Klauda, R. M. Venable, J. A. Freites, J. W. O'Connor, D. J. Tobias, C. Mondragon-Ramirez, I. Vorobyov, A. D. MacKerell Jr and R. W. Pastor, *J. Phys. Chem. B*, 2010, **114**, 7830.
48 A. D. J. MacKerell, D. M. Bashford, R. L. Dunbrack, J. D. Evanseck, M. J. Field, S. Fischer, J. Gao, H. Guo, S. Ha, D. Joseph-McCarthy, L. Kuchnir, K. Kuczera, F. T. K. Lau, C. Mattos, S. Michnick, T. Ngo, D. T. Nguyen, B. Prodhom, W. E. I. Reiher, B. Roux, M. Schlenkrich, J. C. Smith, R. Stote, J. Straub, M. Watanabe, J. Wiórkiewicz-Kuczera, D. Yin and M. Karplus, *J. Phys. Chem. B*, 1998, **102**, 3586.
49 A. A. Petruk, S. Varriale, M. R. Coscia, L. Mazzarella, A. Merlino and U. Oreste, *Biochim. Biophys. Acta, Biomembr.*, 2013, **1828**, 2637.
50 T. Darden, D. York and L. Pedersen, *J. Chem. Phys.*, 1993, **98**, 10089.
51 H. Ellens, J. Bentz and F. C. Szoka Jr, *Biochemistry*, 1984, **23**, 1532.
52 A. Merlino, G. Vitiello, M. Grimaldi, F. Sica, E. Busi, R. Basosi, A. M. D'Ursi, G. Fragneto, L. Paduano and G. D'Errico, *J. Phys. Chem. B*, 2012, **116**, 401.

53 G. Vitiello, S. Di Marino, A. M. D'Ursi and G. D'Errico, *Langmuir*, 2013, **29**, 14239.
54 C. M. Miller, A. C. Brown and J. Mittal, *J. Phys. Chem. B*, 2014, **118**, 13169.
55 R. Spadaccini, G. D'Errico, V. D'Alessio, E. Notomista, A. Bianchi, M. Merola and D. Picone, *Biochim. Biophys. Acta, Biomembr.*, 2010, **1798**, 344.
56 A. Labillov, R. T. Youker, J. R. Bruns, I. Kukic, K. Kiselyov, W. Halfter, D. Finegold, S. J. H. do Monte and O. A. Weisz, *Mol. Genet. Metab.*, 2014, **111**, 184–192.
57 M. Hirai, R. Kimura, K. Takeuchi, M. Sugiyama, K. Kasahara, N. Ohta, B. Farago, A. Stadler and G. Zaccai, *Eur. Phys. J. E: Soft Matter Biol. Phys.*, 2013, **36**, 74.
58 S. Galdiero, A. Falanga, G. Morelli and M. Galdiero, *Biochim. Biophys. Acta, Biomembr.*, 2010, **1848**, 16.